Sanjaya K. Pradhan
e-mail: spradh1@uic.edu

Sudip K. Mazumder
e-mail: mazumder@ece.uic.edu

Laboratory for Energy and Switching-Electronics Systems,
Department of Electrical and Computer Engineering,
University of Illinois at Chicago,
851 S. Morgan Street, MC: 154, 1020 SEO,
Chicago, IL 60607-7053

Joseph Hartvigsen
e-mail: jjh@ceramatec.com

Michele Hollist
e-mail: mhollist@ceramatec.com

SOFC and Hydrogen Technologies,
Ceramatec, Inc.,
Salt Lake City, UT

Effects of Electrical Feedbacks on Planar Solid Oxide Fuel Cell

Planar-solid-oxide-fuel-cell stacks (PSOFCSs), in PSOFC-based power-conditioning systems (PCSs), are subjected to electrical feedbacks due to the switching power electronics and the application loads. These feedbacks (including load transient, current ripple due to load power factor and inverter operation, and load harmonic distortion) affect the electrochemistry and the thermal properties of the planar cells thereby potentially deteriorating the performance and reliability of the cells. In this paper, a detailed study on the impact of these electrical effects on the performance of the PSFOC is conducted. To analyze the impact of such feedbacks, a spatiotemporal numerical system model is developed on a low-cost Simulink modeling platform and the model under transient and steady-state conditions is validated experimentally. Using this validated model, parametric analyses on the impacts of transience, power factor, and distortion of the application load as well as low-frequency current ripple is conducted. Finally, using experimental data, we demonstrate the long-term impact of two most significant electrical feedbacks on the area-specific resistance and the corresponding loss of effective stack power.
[DOI: 10.1115/1.2713773]

Keywords: planar solid oxide fuel cell (PSOFC), modeling, experimental validation, electrical feedbacks, load transients, ripple, power factor, total harmonic distortion (THD), power electronics, power conditioning

1 Introduction

[1]Planar solid oxide fuel cells (PSOFCs) are promising candidates for future alternative-energy-based power systems because of their high energy-conversion efficiency, high fuel flexibility, and tolerance to the fuel impurities [1]. However, the high cost of production and issues with the reliability have been bottlenecks in the commercialization of the PSOFC and PSOFC-based power-conditioning system (PCS) as well.

Several studies have addressed the issues related to the reliability of SOFC. Effects of higher operating temperature and high fuel utilization on the material properties of SOFC have been reported earlier [2,3]. These studies on SOFC have primarily focused on studying the effects of material properties and electrokinetics of chemical reactions on cell operating life and performance. However, there is a need to study the impact of the electrically induced feedback effects (induced due to the power electronics subsystem (PES) and the application loads (AL)) on the PSOFC performance. Achenbach [4] and Hartvigsen et al. [5] have demonstrated preliminary results on the impacts of linear electrical load impedance and their change on the dynamics of a SOFC. Acharya et al. [6,7] and Mazumder et al. [8] have demonstrated effects on the performance and durability of a *tubular* SOFC (TSOFC) stack. Recently, Gemmen [9] attempted to estimate the effects of electrical loads and inverter current ripple on the performance of *proton-exchange membrane* (PEM) fuel cells using a simple first-order model of a PES. As investigated in [6,8,9], the DC-AC inverter ripple currents may have a degrading impact on the fuel cell performance if not adequately controlled.

However, no study had been reported to estimate the effects of such electrical feedbacks on the *planar* SOFC. Again, the impact of several other electrical feedbacks, such as the load power factor, harmonic distortion, and the nature of load transients on the performance and reliability of any fuel cell system, are not investigated. Therefore, in this paper, using a transient system model comprising a two-dimensional (2D) and spatiotemporal PSOFC model and a nonlinear PES model, we investigate the impacts of PES- and AL-induced electrical effects on the performance of the PSOFC. The steady-state and transient predictions of the cell model are experimentally validated. Subsequently, using this validated model, parametric analyses on the impacts of transience, power factor, and distortion of the application load as well as low-frequency current ripple is conducted. Finally, we demonstrate (experimentally) the long-term impact of two most significant electrical feedbacks on the area-specific resistance and the corresponding loss of effective stack power.

2 Electrical Feedbacks

We consider two types of electrical feedbacks: those that are induced by the power electronics and those that are induced by the application load.

2.1 Power-Electronics-Induced Feedbacks

2.1.1 Low-Frequency Ripple. A single-phase fuel cell DC-AC converter (also known as inverter as shown in Fig. 1) for stationary application feeds an AC load at line frequency, which is 60 Hz in the USA and 50 Hz in Europe. The AC current drawn by the load from the inverter introduces ripple in the current drawn from the fuel cell. This low-frequency ripple current (with a frequency that is twice that of the line frequency) increases with an increase in the load current. Figure 2 illustrates the low-frequency ripple in the PSOFC-stack (PSOFCS) current. As shown in Sec. 2.2.2 and 2.2.3, the ripple current is also dependent on the power factor and load distortion. Because the electrochemical time constant of the PSOFCS is less than the time period of the ripple, the low-frequency ripple current may potentially affect the electrochemical properties of the stack, such as the fuel utilization in the stack and the current density.

2.1.2 High-Frequency Ripple. High-frequency ripple usually refers to the switching ripple of the PES and is typically over

[1]A PSOFC-based PCS essentially consists of a PSOFC stack, a balance-of-plant subsystem (BOPS), which controls the flow of fuel and air into the stack and as well controls the stack temperature, and power electronics subsystem (PES), which processes the output power from the stack, and provides an interface between the stack and the application load (AL).

Submitted to ASME For Publication in the Journal of Fuel Cell Science and Technology Manuscript received April 19, 2006; final manuscript received July 17, 2006. Review conducted by Masashi Mori.

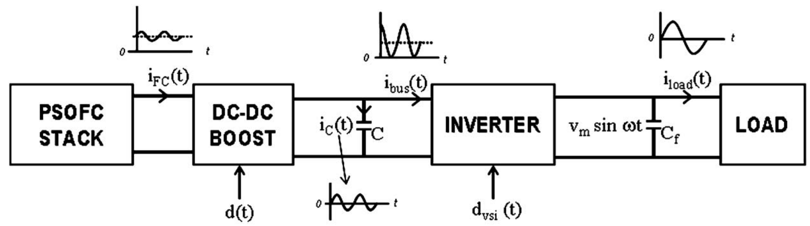

Fig. 1 Schematic of a PSOFC based residential power-conditioning system

10 kHz. It has an impact on the electrochemical impedance and efficiency of the PSOFC. However, because the time period of the high-frequency ripple is much smaller compared to the electrochemical time constant of the planar fuel cell, it may have negligible impact on the performance of the planar cell. Figure 2 illustrates high-frequency ripple in the current drawn from the PSOFC stack.

2.2 Load-Induced Feedbacks. One of the most commonly observed load-induced feedbacks is the *load transient*, which is attributed to sudden variation in the power demand of the load or its sudden isolation from the fuel cell stack. Other important feedback effects are the *power factor* of the load and its *harmonic distortion*, both of which are indicative of the quality of the load.

2.2.1 Load Transients. The load current transients occur due to the variations in the power demands of the load. Because PSOFC (like other fuel cells) is not a stiff voltage source, its voltage level decreases with an increase in the current drawn from it. This is due to an increase in the polarization loss at a higher current density. For the PSOFC, operation below a minimum voltage should be avoided because the mass-transport limitations of the electrochemical reaction can cause the anode of the cell to be reoxidized. This degrades the cell performance and ultimately shortens the life of the stack. Hence, load transients, which may drop the voltage of the PSOFC below this minimum voltage, can degrade the performance and durability of the stack.

2.2.2 Load Power Factor. For a passive ac load, load power factor (which can vary between 0 and 1), as illustrated in Fig. 3(*a*), represents the phase difference between the voltage across a load and the current drawn by it. When the load is resistive, it draws only active power from the source, and hence, the power factor is unity. However, at nonunity power factors, an ac load draws both reactive and active powers from the source. The reactive power ($P_{\text{reactive}}(t)$), as shown in Fig. 3(*b*), circulates in the circuit. To support $P_{\text{reactive}}(t)$, additional reactive current is drawn from the source apart from the active current (which feeds active power to the load). The higher the magnitude of this ac current the higher is the magnitude of the ripple in the current drawn from the dc source. As explained in the Appendix B, the lower the power factor the higher the magnitude of the fuel cell ripple current.

2.2.3 Total Harmonic Distortion (THD). Total harmonic distortion signifies the harmonic content in an ac quantity, and is defined as the ratio of sum of powers of all harmonic frequency components in a signal above the fundamental frequency to the power of the fundamental frequency component. An AC-DC rectifier load is a typical example of the load that induces harmonic distortion to the AC current at the output of the inverter (refer to Fig. 1). As shown in Fig. 4(*a*), current drawn from the inverter, $i(t)$, is distorted. The harmonic analysis of the distorted current, as shown in Fig. 4(*b*), reveals the presence of the significant odd-order harmonics that decreases with increase in the frequency. The analysis of the harmonics in the load in the Appendix D, concludes that the magnitude of the ripple in the current drawn from the bus, $i_{\text{bus}}(t)$, and therefore in the current drawn from the PSOFC stack, $i_{\text{FC}}(t)$, are dependent on the power factor of the fundamental load current and the fractions of harmonic contents in the load.

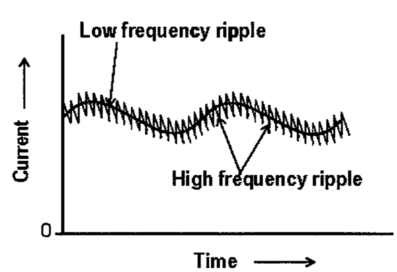

Fig. 2 Power-electronics induced high- and low-frequency ripples in the fuel cell current

3 Modeling and Validation

For an accurate estimation of the impact of the electrical feedbacks, a comprehensive modeling framework for a PSOFC PCS is

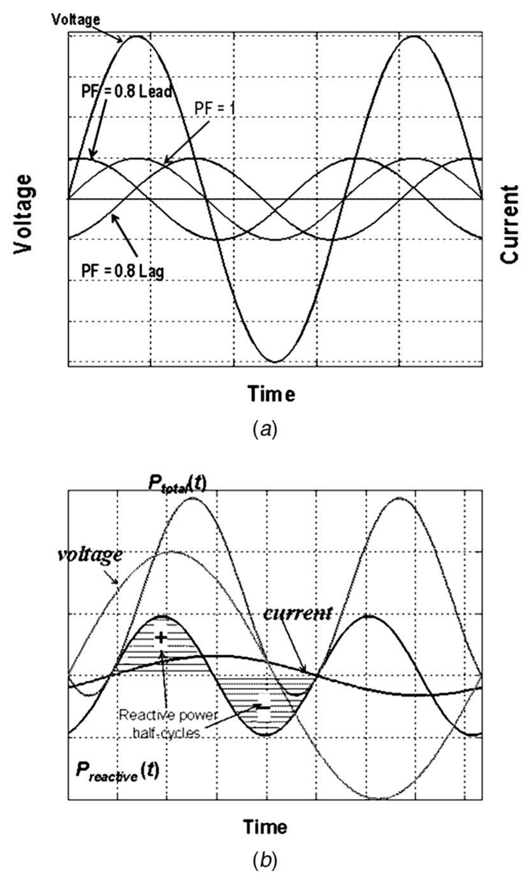

Fig. 3 (*a*) Voltage-current (*V-I*) characteristics of AC loads at different power factors and (*b*) illustration of the circulating reactive power due to nonunity power factor of the load

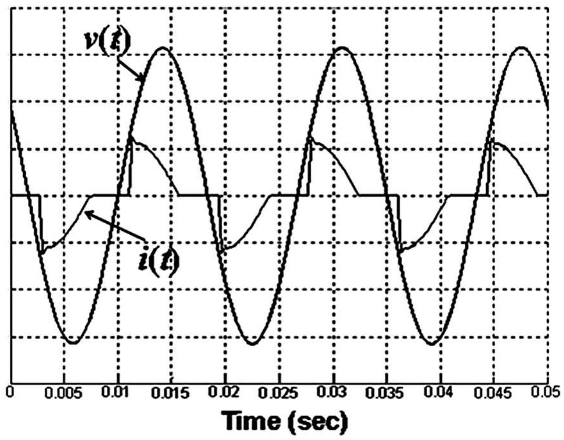

(*a*)

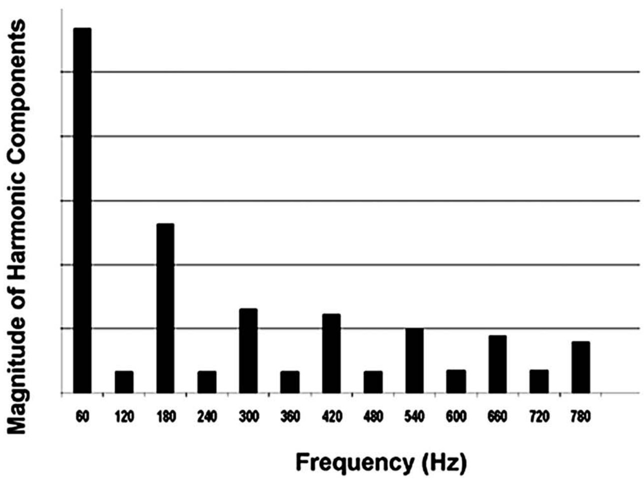

(*b*)

Fig. 4 (*a*) Current distortion due to a rectifier load and (*b*) Fourier analysis of the distorted current

built, which can potentially address the key issues, including resolving the interactions among PSOFC, power electronics subsystem (PES), and application load (AL) and enable parametric system studies. The comprehensive numerical model requires low-cost SIMULINK/MATLAB, including SIMPOWERSYSTEM for implementation, and comprises the spatiotemporal PSOFC stack subsystem implemented in MATLAB/SIMULINK, and the PES and AL profile implemented in SIMPOWERSYSTEM in SIMULINK.

3.1 PSOFC Model

3.1.1 Two-Dimensional PSOFC Model. For accurate prediction of the effects of system interactions on the PSOFC, one needs to analyze the PSOFC internal parametric variations [10–14]. A spatiotemporal electrothermochemical model of the PSOFC is developed in SIMULINK, which provides spatial discretizations of the cell. This model is designed to accept required system inputs (reactant stream flow rates and compositions, temperatures, cell geometric parameters, and cell current) and computes spatial properties, such as cell current density, across an entire planar cell surface.

The cell temperature (T) in the two-dimensional (x and y) model, as shown in Fig. 5, is computed from the time-dependent solution of the following equation:

$$\rho C_p \frac{\partial T}{\partial t} - k\left(\frac{\partial T^2}{\partial x^2} + \frac{\partial T^2}{\partial y^2}\right) = Q \tag{1}$$

$$Q = \left(\frac{V_{tn} - V_{op}}{l}\right) j + (-\Delta H_{\text{shift}}) \tag{2}$$

$$V_{tn} = -\frac{\Delta H}{nF} \tag{3}$$

where V_{tn} is the thermal neutral voltage, V_{op} is the operating voltage, j is the current density, ρ is the mass density of the control volume, C_p is the combined specific heat at constant pressure, l is the cell thickness, ΔH_{shift} is the enthalpy of the shift reaction in the control volume, ΔH is the enthalpy of the main reaction, n is the molar flow rate of the fuel, and k is the thermal conductivity of

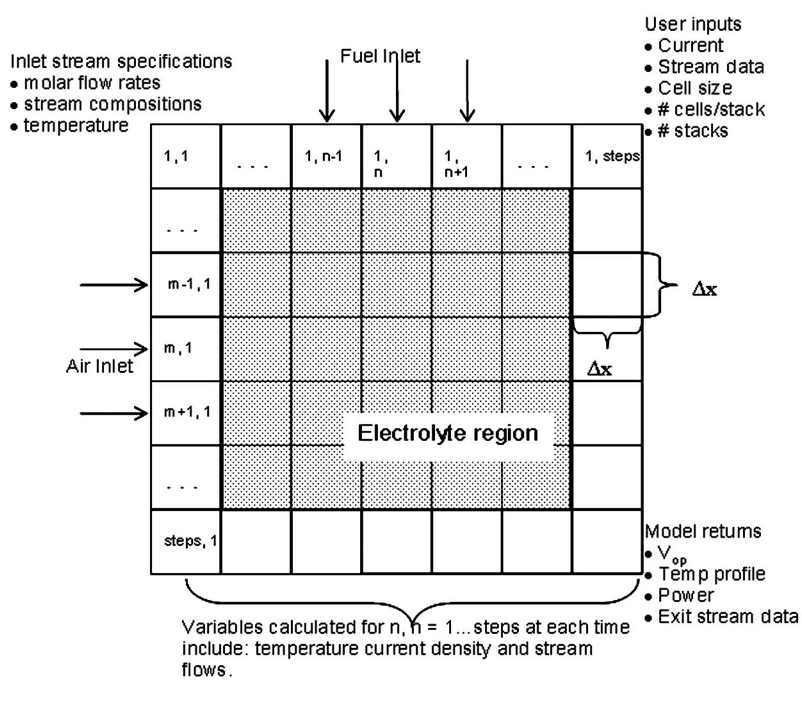

Fig. 5 Spatial homogenous model for the PSOFC providing two-dimensional discretizations; electrolyte region signifies electro-active area of the cell

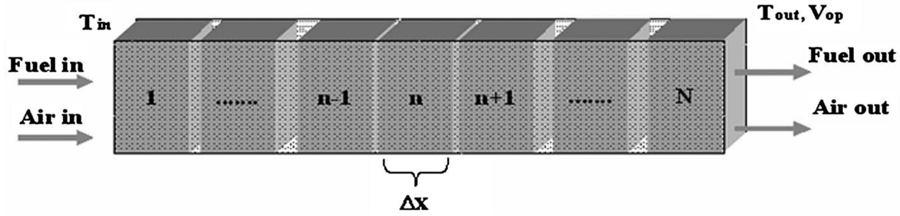

Fig. 6 One-dimensional homogenous slab model for PSOFC providing discretizations involving finite-difference method; Temperature, current, and molar-flow rates of air and fuel are calculated each time for $n=1,\ldots,N$

the fuel cell. To approximate the second-order partial-differential equation, a finite-difference method using central differences [15] is used,

$$\frac{\partial T^2}{\partial x^2} \approx \frac{1}{\Delta x^2}[T_{m+1,n,t} - 2T_{m,n,t} + T_{m-1,n,t}] \quad \text{and}$$

$$\frac{\partial T^2}{\partial y^2} \approx \frac{1}{\Delta y^2}[T_{m,n+1,t} - 2T_{m,n,t} + T_{m,n-1,t}] \tag{4}$$

By approximating $\partial T/\partial t$ as a simple forward difference and substituting $[(T_{j+1}-T_j)/\Delta t]$ for $\partial T/\partial t$, substituting (2) into (1), and marching the solution through time yields the Euler's explicit-integration scheme for the determination the spatial temperature variation. With the step size $\Delta x=\Delta y$, the expression for temperature becomes

$$T_{m,n,t+1} = \frac{k\Delta t}{\rho C_p \Delta x^2}(T_{m-1,n,t} + T_{m,n-1,t} + T_{m,n+1,t} + T_{m+1,n,t} - 4T_{m,n,t}) + T_{m,n,t} + \frac{\Delta t}{\rho C_p}Q \tag{5}$$

In the course of each of the iteration, the assumed operating voltage is used to determine the current density in each of the control volumes throughout the cell using

$$j_{m,n} = \frac{En_{m,n} - V_{op}}{\mathrm{ASR}_{m,n}} \tag{6}$$

where $\mathrm{ASR}_{m,n}$ is the local temperature-dependent area-specific resistance and $En_{m,n}$ is the Nernst potential defined as

$$En_{m,n} = -\frac{\Delta G}{nF} \tag{7}$$

ΔG is the change in the Gibb's free energy. The current density as in (6) is then summed to compute the total cell current,

$$I = \sum_{m=1}^{\text{steps}} \sum_{n=1}^{\text{steps}} \frac{\Delta x \Delta y(En_{m,n} - V_{op})}{\mathrm{ASR}_{m,n}} \tag{8}$$

The local current-density values are used to determine the change in stream composition based on the electrochemical reaction in each control volume. The fuel exit composition of each control volume is equilibrated with respect to the shift reaction before entering the downstream control volume.

3.1.2 One-Dimensional PSOFC Model. To reduce the computational complexity of the spatial PSOFC model, a one-dimensional (1D) model based on homogeneous slab model for the PSOFC (as shown in Fig. 6) is derived from its two-dimensional form (i.e., Eqs. (1)–(8)) by discretizations only in one dimension (x). The model based on coflow of air and fuel computes various parameters at discrete segments along the length of the planar cell.

The summary of the equations of the one-dimensional PSOFC model is as follows:

$$\rho C_p \frac{\partial T}{\partial t} - k\frac{\partial T^2}{\partial x^2} = Q$$

$$V_{tn} = -\frac{\Delta H}{nF}$$

$$T_{n,t+1} = T_{n,t} + \frac{k\Delta t}{\rho C_p \Delta x^2}(T_{n+1,t} - 2T_{n,t} + T_{n-1,t}) + \frac{\Delta t}{\rho C_p}Q$$

$$En_n = -\frac{\Delta G}{nF}$$

$$Q = \left(\frac{V_{tn} - V_{op}}{1}\right)j_n + (-\Delta H_{\text{shift}})$$

$$\frac{\partial T^2}{\partial x^2} \approx \frac{1}{\Delta x^2}[T_{n+1,t} - 2T_{n,t} + T_{n-1,t}]$$

$$j_n = \frac{(En_n - V_{op})}{ASR_n}$$

$$I = \sum_{n=1}^{\text{steps}} \frac{\Delta x^2(En_n - V_{op})}{\mathrm{ASR}_n}$$

3.2 PES Model. The voltage of the *planar* SOFC stack varies with current drawn by the load, decreasing significantly at higher load currents. Therefore, a PES is needed to process the raw output power from the stack and provide power to the load at constant DC or AC voltage. The topological model of PES for a residential power system is shown in Fig. 7. The model consists of a DC-DC (boost) converter to step up the PSOFC output voltage to a higher intermediate dc bus voltage. The operation and control of DC-DC boost converter is defined and explained in detail in [16]. A DC-AC converter (inverter) is further used to convert the output of the DC-DC boost converter, to feed the AC load. For this purpose, a pulse-width-modulated voltage source inverter

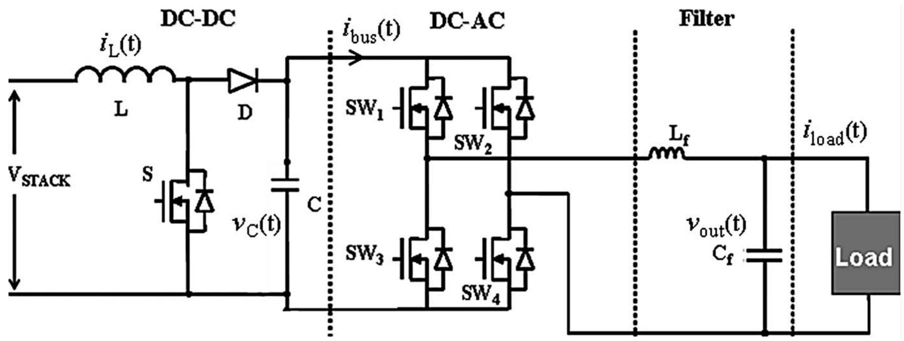

Fig. 7 A simplified architecture of the PES for the residential PCS

(VSI) is used, due to its simpler control scheme. The high-frequency harmonic content of the output of the VSI is eliminated by the output filter. The operation and control of full-bridge VSI is defined and explained in detail in [17]. The chosen topology of the PES enables the study of the impacts on the SOFC stack due to low-frequency ripple current.

Typically, PES is a piecewise linear (PWL) systems, whose state-space equations can be expressed as

$$\dot{\mathbf{x}}(t) = A_i\mathbf{x}(t) + B_i\mathbf{u}(t) + C_i\mathbf{v}(t) \tag{9}$$

where $\mathbf{x}(t) \in \Re^n$ are the states of the system, $\mathbf{u}(t) \in \Re^n$ and $\mathbf{v}(t) \in \Re^m$ represent the input and the output vector of the system, respectively. The matrices A_i, B_i, and C_i describe the dynamics of the state-space model for the ith switching state of the system. The sequence and the duration of the switching states are governed by the closed-loop controller of the system.

As an illustration, the DC-DC boost converter can be modeled using (9) as

$$\dot{\mathbf{x}}_1 = A_1\mathbf{x}_1 + B_1u_1 + C_1v_1 \tag{10}$$

where, $\mathbf{x}_1$ represents the state vector, given as $[i_Lv_C]^T$, u_1 is the input of the system, which is the stack voltage, V_{stack}, and $\mathbf{v}_1$ is the system output, that is i_{bus}. When the switch S of the boost converter is turned ON, the energy content in the inductor L increases, and the system of Eq. (10) becomes

$$\dot{\mathbf{x}}_1 = \begin{bmatrix} 0 & 0 \\ 0 & 0 \end{bmatrix}\mathbf{x}_1 + \begin{bmatrix} \frac{1}{L} \\ 0 \end{bmatrix}u_1 + \begin{bmatrix} 0 \\ \frac{1}{C} \end{bmatrix}v_1 \tag{11a}$$

And when the switch S is turned OFF, the stored energy in the inductor is transferred to the output capacitor C of the converter through the diode D and Eq. (10) becomes

$$\dot{\mathbf{x}}_1 = \begin{bmatrix} 0 & -\frac{1}{L} \\ \frac{1}{C} & 0 \end{bmatrix}\mathbf{x}_1 + \begin{bmatrix} \frac{1}{L} \\ 0 \end{bmatrix}u_1 + \begin{bmatrix} 0 \\ -\frac{1}{C} \end{bmatrix}v_1 \tag{11b}$$

Therefore, the DC-DC boost converter as shown in Fig. 8 can be completely described as

$$\dot{\mathbf{x}}_1 = \begin{bmatrix} 0 & -\frac{\bar{s}}{L} \\ \frac{\bar{s}}{C} & 0 \end{bmatrix}\mathbf{x}_1 + \begin{bmatrix} \frac{1}{L} \\ 0 \end{bmatrix}u_1 + \begin{bmatrix} 0 \\ \frac{1}{C} \end{bmatrix}v_1 \tag{12}$$

where the switching function s [$\bar{s}$=NOT(s)] represents the turn ON and turn OFF states of the switch S. The switching function is determined to obtain the required bus voltage.

Similarly the VSI, as shown in Fig. 7, can be modeled as in (9) as

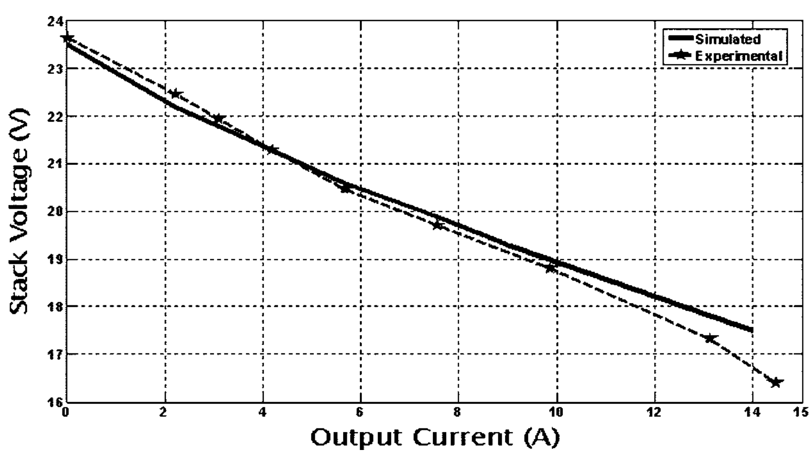

Fig. 8 Steady-state I-V characteristics comparison of the planar SOFC stack

$$\dot{\mathbf{x}}_2 = A_2\mathbf{x}_2 + B_2u_2 + C_2v_2 \tag{13}$$

where $\mathbf{x}_2$ represents the state vector, given as $[i_{\text{bus}}v_{\text{out}}]^T$ and u_2 is the system input and is given as $\nu_C(t)$, and v_2 is the system output representing the load current, $i_{\text{load}}(t)$. The switch pairs SW_1-SW_3 and SW_2-SW_4 switch in complement with a small time delay between the switching OFF of SW_1 (SW_3) and switching ON of SW_2 (SW_4). This time delay provides a zero state for the voltages and currents (voltage and currents in this state remain ideally unchanged, assuming no loss). The time delay, which is kept at half of the switching period for symmetry, effectively doubles the frequency of the harmonics. This leads to reduction in the harmonics in the output voltage.

When the switch pair SW_1-SW_3 turn ON, (13) becomes

$$\dot{\mathbf{x}}_2 = \begin{bmatrix} 0 & \dfrac{-1}{L_f} \\ \dfrac{1}{C_f} & 0 \end{bmatrix}\mathbf{x}_2 + \begin{bmatrix} \dfrac{1}{L_f} \\ 0 \end{bmatrix}u_2 + \begin{bmatrix} 0 \\ -\dfrac{1}{C_f} \end{bmatrix}v_2 \tag{14a}$$

When the switch pair SW_2-SW_4 turned ON, the system of Eq. (13) becomes

$$\dot{\mathbf{x}}_2 = \begin{bmatrix} 0 & \dfrac{1}{L_f} \\ \dfrac{-1}{C_f} & 0 \end{bmatrix}\mathbf{x}_2 + \begin{bmatrix} \dfrac{1}{L_f} \\ 0 \end{bmatrix}u_2 + \begin{bmatrix} 0 \\ -\dfrac{1}{C_f} \end{bmatrix}v_2 \tag{14b}$$

The overall VSI as shown in Fig. 7 can be described as

$$\dot{\mathbf{x}}_2 = \begin{bmatrix} 0 & \dfrac{-s_a+s_b}{L_f} \\ \dfrac{s_a-s_b}{C_f} & 0 \end{bmatrix}\mathbf{x}_2 + \begin{bmatrix} \dfrac{1}{L_f} \\ 0 \end{bmatrix}u_2 + \begin{bmatrix} 0 \\ -\dfrac{1}{C_f} \end{bmatrix}v_2 \tag{15}$$

The switching function $\mathbf{s}$ of the VSI is given as $\mathbf{s}=[s_a s_b]$, where s_a represent the ON state of the SW_1-SW_3 pair and s_b represents the ON state of the SW_2-SW_4 pair. The ON time of s_a and s_b are generated by a sinusoidally modulated switching sequence to obtain an averaged sine wave ac at the output of the VSI. Combining Eqs. (12) and (15), the complete PES system as in Fig. 7 can be expressed as

$$\dot{\mathbf{X}} = \begin{bmatrix} 0 & \dfrac{-\bar{s}}{L} & 0 & 0 \\ \dfrac{\bar{s}}{C} & 0 & \dfrac{-1}{C} & 0 \\ 0 & \dfrac{1}{L_f} & 0 & \dfrac{-s_a+s_b}{L_f} \\ 0 & 0 & \dfrac{s_a-s_b}{C_f} & 0 \end{bmatrix}\mathbf{X} + \begin{bmatrix} \dfrac{1}{L} \\ 0 \\ 0 \\ 0 \\ 0 \end{bmatrix}U + \begin{bmatrix} 0 \\ 0 \\ 0 \\ \dfrac{-1}{C_f} \end{bmatrix}V \tag{16}$$

where $\mathbf{X}=[i_L\, v_C\, i_{\text{bus}}\, v_{\text{out}}]^T$ is the state vector, the stack voltage V_{stack} represents the system input U, and the output load current i_L is the output of the system.

3.3 Model Validation. The effect of electrical feedbacks on PSOFCs is studied on the stack prototype, as shown in Fig. 9(*a*), consisting of 25 planar cells in series. In the stack, all the planar cells are mounted in a single manifold. The cross-flow arrangement for the reactants in the stack is illustrated in Fig. 9(*b*). Each cell has an electroactive area of 64 cm^2. The detail specification and the test condition of the stack are given in Appendix A.

These specifications and test conditions are set as the input to the 1D and 2D models. The ASR of the individual PSOFC for the models at any core temperature are obtained using the empirical formula

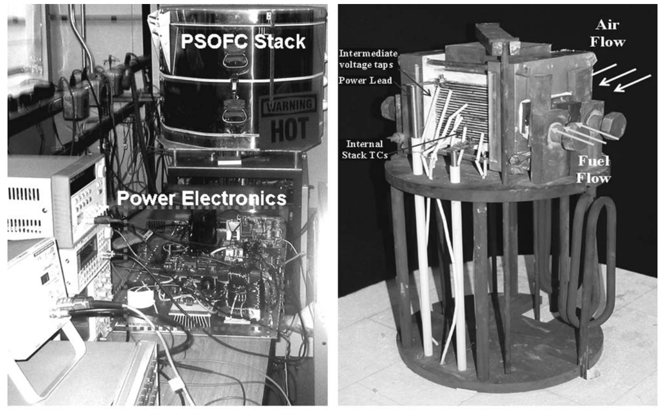

(*a*) (*b*)

Fig. 9 (*a*) Experimental setup of the 25 cell PSOFC stack with the PES; the flow of air and fuel into the stack is kept constant and (*b*) The PSOFC stack manifold and the arrangements for air and fuel flow

$$\text{ASR} = Ae^{B/T} \tag{17}$$

where T is the stack core temperature, which depends on the flow rates and temperature of the inlet gases and the stack fuel utilization, the constants A and B are obtained experimentally from the stack characteristics. Similarly, the 1D and 2D model calculates the specific heat capacity and cell density based on the core temperature and experimentally determined constants (refer to Appendix A).

Comparison of I-V characteristics of the 25 cell stack model and the 25 cell stack experimental unit, as shown in Fig. 8, shows the accuracy of the model in the steady state. The response of the model is again verified during several electrical feedbacks to prove its accuracy even in the strictest of the transients.

3.3.1 Load Transients. We analyze the effects of load transient on the output of the PSOFC stack. A programmable electronic load operating in constant current mode is connected across the stack output, and a current transient of 2.2 A to 12 A, and subsequently, 12 A to 2.2 A is applied after 1400 s. Figures 10(*a*) and 10(*b*) show the drop in the output voltage of the stack model and the experimental stack prototype, respectively. The voltage drop is attributed to the enhanced polarization losses owing to a surge in the current density. Because of the subjected load transient, the mean temperature in the stack increases as shown in Fig. 11(*a*).

(The mean temperature profile near the no-load to full-load transient is skewed due to manual turning off of the electronic load at $t=2000$ s, accidentally.) The increase in the stack temperature is attributed to the increased rate of the exothermic reaction. However, the thermal time constant of the stack being much larger than that of the SOFC electrochemistry/PES time constant, the cell temperature gradually reaches the steady state value after ~600 s.

To investigate the effect of multiple load transient, we subject the system to multiple small duration loads. The duration of the load is kept fixed at 300 s followed by 300 s of no load condition. Because of the multiple set of transient load, the temperature of the PSOFC does not have sufficient time to drop back to its initial value as shown in Fig. 11(*b*). Hence, the multiple load transients may lead to a higher temperature inside the PSOFC.

3.3.2 Ripple. The effect of the ripple is studied using a power electronics prototype, which consists of a bidirectional DC-DC boost converter connected across the stack. The duty ratio of switches of the converter is modulated using a sinusoidal signal of 60 Hz, producing 60 Hz AC voltage at the output. The current drawn from the stack contains 120 Hz ripple. The load connected

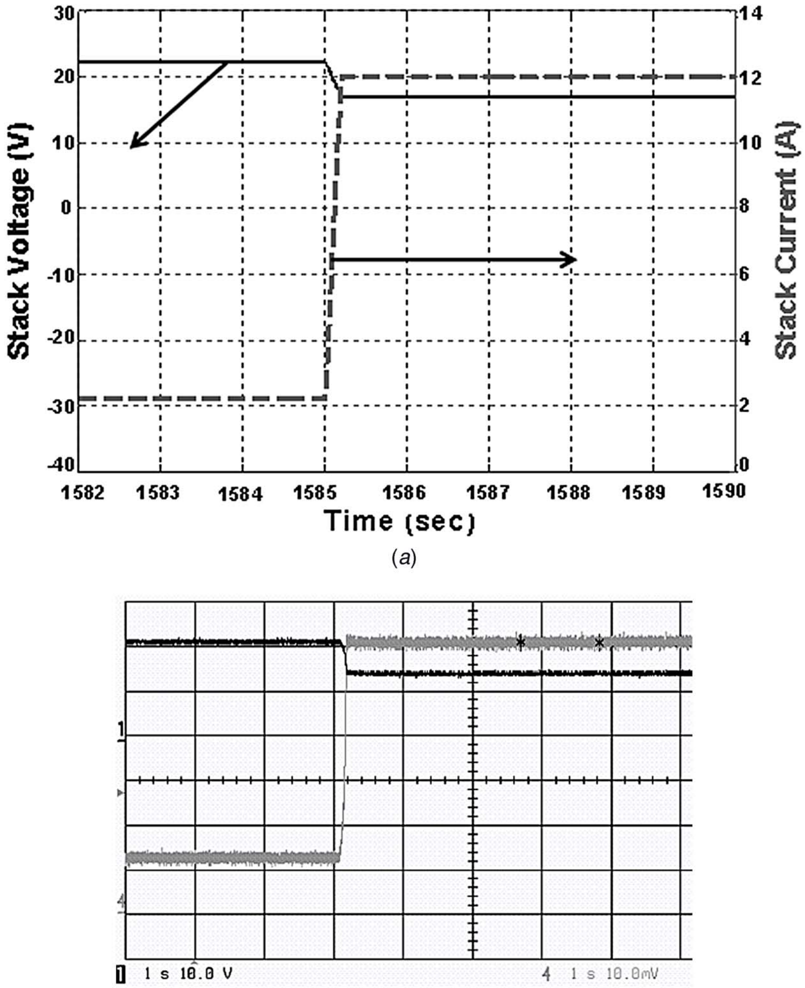

(*a*)

(*b*)

Fig. 10 (*a*) Effect of load current transient (2.2–12 A) on the voltage of the stack model and (*b*) the experimental validation of its effect on the planar stack, scope channel 1 (10 V/div) and channel 4 (2 A/div) measures the stack voltage and current, respectively

across the boost converter is adjusted so that the magnitude of the ripple is 40% of the mean stack current. Figures 12(*a*) and 12(*b*) show the effect of a low-frequency (120 Hz) ripple on the 1D stack model and the experimental prototype, respectively.

4 Parametric Analysis of the Effects of Electrical Feedbacks

To analyze the impacts of several electrical feedbacks, the validated model is subjected to the feedbacks of various amplitude and/or frequency. And, their effects on the performance and durability of the stack are evaluated based on their effect on the change in the mean temperature and the fuel utilization.

4.1 Effect of Load Transient. The level of increase in the mean temperature of the stack is found to be dependent only on the initial and the final load current drawn from the stack and is independent of the slew rate of the load current during the transient. Figure 13(*a*) shows the increase in the mean temperature, based on the percentage of the load current. However, as shown in Fig. 13(*b*), the effect of the slew rate of the load transient on the temperature is negligible. As the frequency of the occurrence of the load transient increases, the stack gets less and less time to cool down, leading to a residual increase in the stack temperature. Figure 13(*c*) shows the effect of the multiple load transients on the stack temperature.

4.2 Effect of Ripple. Fuel utilization, which is defined as the fraction of the incoming fuel utilized, is directly proportional to the current drawn from the stack at a constant fuel flow rate. Maximum operable fuel utilization is the ideal fuel utilization level to achieve peak stack efficiency, assuming uniform distribution of fuel through out the stack and no fuel loss in the stack. This level is approximately 0.95–0.99.

To draw maximum power from the stack and hence to achieve very high efficiency, the stack must be operated at a particular current level (this corresponds to the maximum operable fuel utilization) as shown in Fig. 14. However, due to the presence of low-frequency ripple in the stack current, the operating mean stack current has to be decreased to avoid zero-reactant condition, as illustrated in Fig. 14. This decrease in the mean stack current decreases the maximum operating stack fuel utilization. Figure 15(*a*) shows the required decrease in the fuel utilization at higher magnitude of the current ripple. Now, with decrease in the fuel utilization level in the stack, the stack efficiency decreases as shown in Fig. 15(*b*).

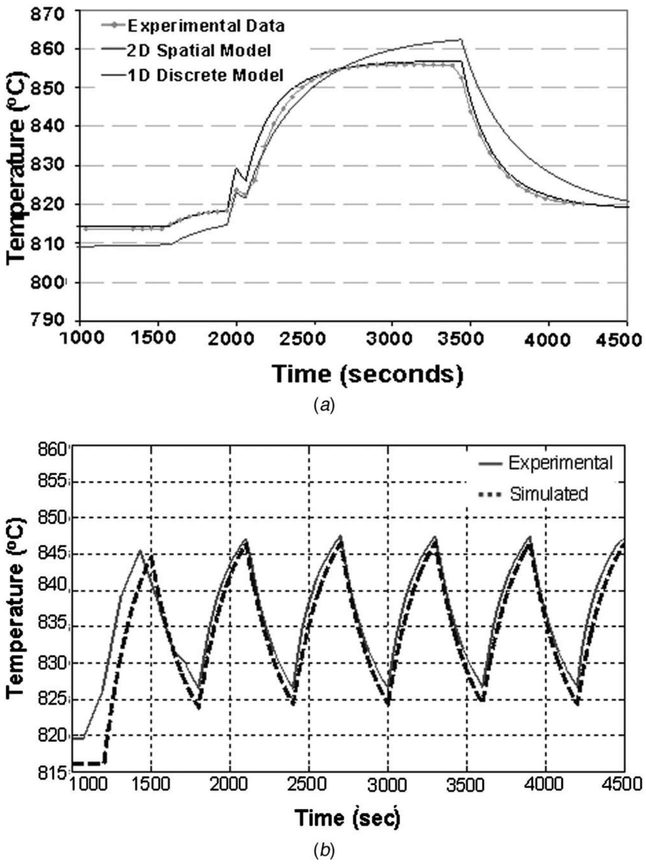

Fig. 11 (***a***) **Validation of the effect of single load transient (no load (NL) –, full load (FL) –, no load (NL)), and (*b*) multiple load transient on the stack temperature**

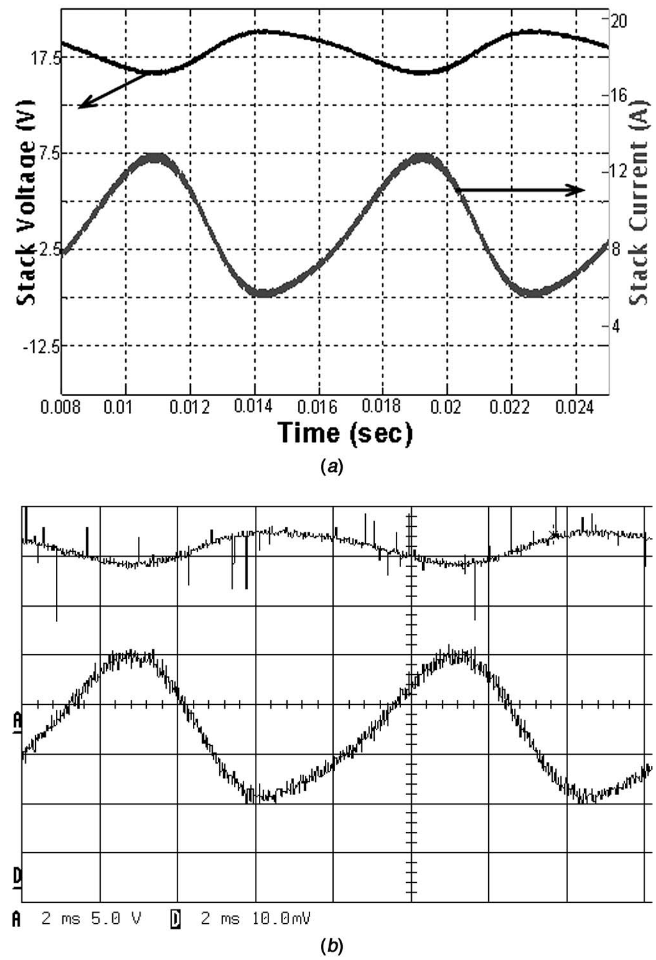

Fig. 12 (***a***) **Effect of 40% current ripple on the stack voltage of 1D model and (*b*) experimental validation of the ripple effect on planar SOFC stack, scope channels A and D show the stack voltage and current, respectively**

Figure 15(*c*) shows the effect of the ripple on the stack temperature. Since the thermal time constant of the planar cell is much higher as compared to the time scale of the low-frequency ripple, the stack temperature would not reflect any variation in a small time scale. The stack temperature depends on the power drawn from the stack. Even with a 100% ripple, the increase in the rms current drawn from the stack is ~5.96%, the increase in the stack current in the steady state is negligible.

4.3 Effect of Load Power Factor. Because of the nonunity power factor of the load, the ripple in the stack current increases (refer to the analysis in Appendix B). This ripple further depends on the output capacitance connected across the DC bus. Figure 16 shows the effect of load power factor variation on the stack current ripple at various capacitances and at a constant active power drawn by the load. As shown in Fig. 14, the available power from the stack decreases with an increase in the current ripple magnitude. Therefore, a decrease in the load power factor decreases the efficiency of the stack. However, as discussed under the effect of the ripple, and since the variation in the power drawn from the stack due to ripple is negligible at various power factor loads drawing the same active power, the increase in the mean temperature should be minimal.

4.4 Effect of THD. An increase in the THD of the ac load increases the distortion in the output ac current due to increase in the magnitude of the harmonic components as well their phase. This distortion in the ac current also introduces distortion in the current drawn from the planar stack. Figure 17 shows the effect of the variation of the THD at different power factors on the ripple magnitude in the stack current. At a fixed power factor of the fundamental current, the percentage ripple in the stack current decreases with an increase in the THD of the load (refer to the analysis and calculation in Appendix C). However, due to minimal variation in the power drawn from the stack, the increase in the mean temperature is minimal.

5 Long-Term Degradation Experiment

To study the effect of two of the important electrical feedbacks in the long term, two set of experimental test beds are built using the similar cells used for the transient experiment. The degradation study of ripple is conducted on a five cell stack connected to a boost converter, and a five cell stack connected to the constant load. The duty ratio of the switch of the boost converter is modulated sinusoidally at 60 Hz. The average current drawn from both the stacks are kept at ~13 A. The open circuit voltage of the five cell stack is 5.087 V. Similarly, for the study the long-term degradation effect due to the load transient, a 25 cell planar stack is connected to a programmable DC-DC converter followed by a load resistance. The DC-DC converter is programmed to draw 13 A current for first 20 min and 2.2 A for the next 10 min in every half-hour. Therefore, the average current drawn from the stack is 9.4 A. The open circuit voltage (V_{oc}) of the stack is 24.75 V. For the five-cell stacks, the flow rates of H_2, N_2, and Air are 1.9 slpm, 0.33 slpm and 7.65 slpm, respectively. The air inlet temperature is kept at 800°C and the core temperature is 850°C.

Figure 18 shows the percentage degradation of the ASR (area-specific resistance) in the stacks after ~900 *h* of study. This

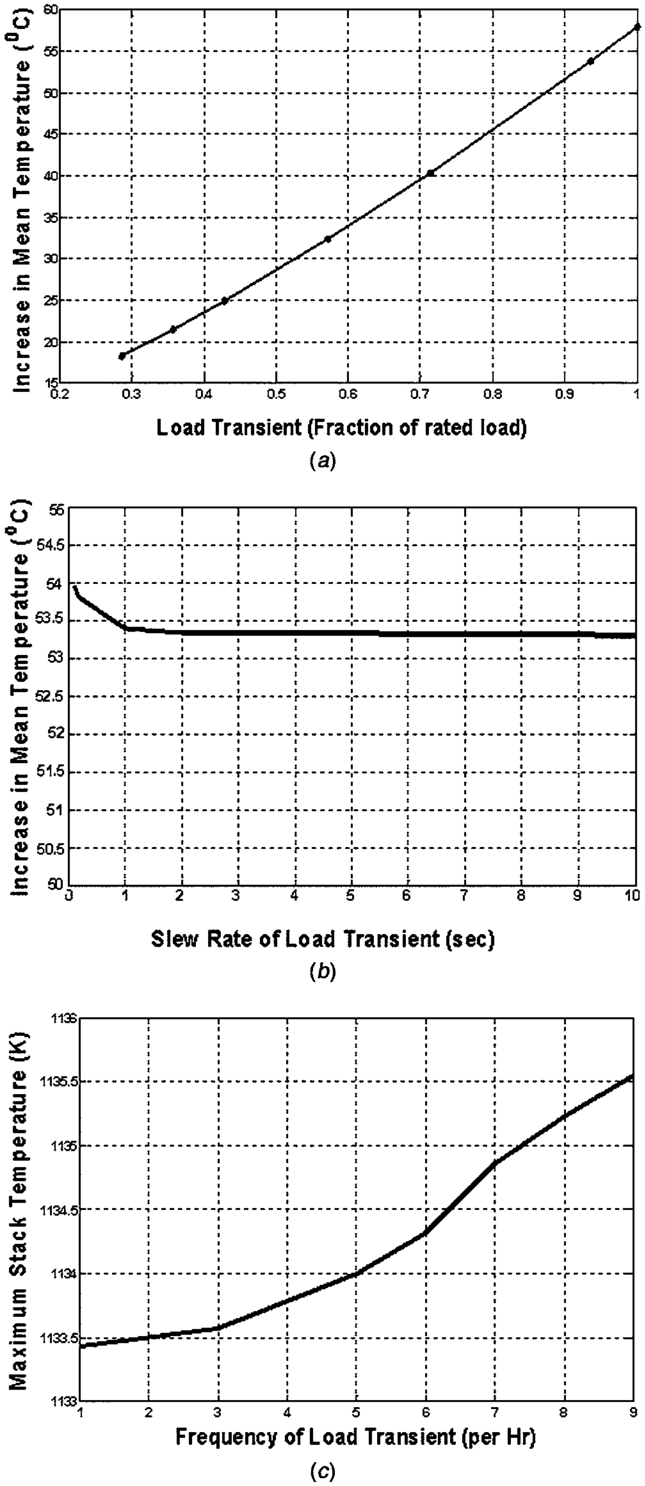

Fig. 13 Effect of (*a*) magnitude of load transient, (*b*) duration of load transient, and (c) the frequency of transients on the increase in the mean stack temperature

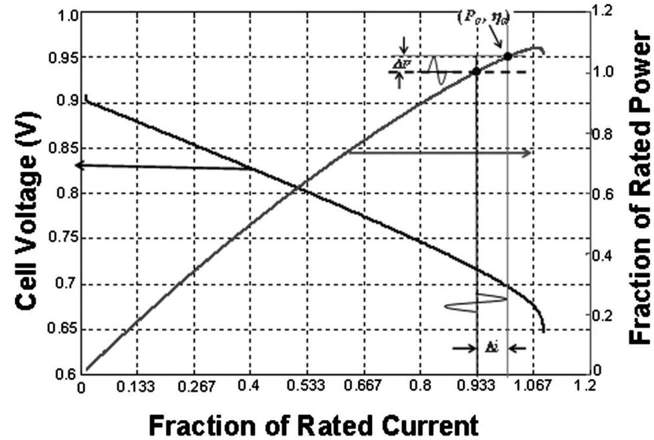

Fig. 14 Effect of low frequency ripple on the performance and efficiency of the stack

shows that, the degradation of the ASR due to the load transient is very high as compared to the stack carrying constant current. Similarly, increase in the ASR of the stack with low-frequency ripple current is higher as compared to the stack feeding constant current.

The degradation in the ASR due to the ripple is found to be 0.06 $\Omega\,\mathrm{cm}^2$ higher as compared to the constant current case after 880 *h* of operation. The increase in the ASR degradation leads to a drop in the power output of the stack. The percentage drop in the output power is given as

$$\Delta P_{\mathrm{drop}} = V_{fc}I_{fc} - V'_{fc}I_{fc} = \left(\frac{(\mathrm{ASR}' - \mathrm{ASR}_b)I_{fc}}{A_{\mathrm{cell}}}\right)I_{fc}$$

$$= (\Delta\mathrm{ASR})\frac{I_{fc}^2}{A_{\mathrm{cell}}} = \frac{\%(\Delta\mathrm{ASR})}{100}\frac{I_{fc}^2}{A_{\mathrm{cell}}}\mathrm{ASR}_b \qquad (18)$$

where I_{fc} is the average current drawn from the fuel cell, A_{cell} is the electroactive area of the planar cell, ASR_b is the base ASR of the stack, and ASR' is the ASR of the stack after degradation. Comparing the efficiencies of the stacks, the stack carrying 100% ripple in the current is found to have an additional drop of 1.72% to that of the stack carrying constant current, and the efficiency of the stack with the load transient drops by 10.32% as compared to the constant current stack.

The analysis of the long-term degradation experiment above indicates that the ASR of the cell degrades with time, when a current is drawn from the stack. However, this degradation is enhanced due to the presence of the ripple in the current and due to the load transients. The degradation of the ASR of the cell deteriorates its efficiency. The load transient, even though at a smaller rate as compared to the frequency of the ripple poses higher threat to the performance and the efficiency of the planar stack.

6 Conclusion

We delineate several different electrical feedbacks induced due to the power electronics subsystem (PES) and the application load (AL), which may potentially affect the performance and durability of planar solid oxide fuel cell stacks (PSOFCSs). To analyze the impact of such feedbacks, a comprehensive, spatiotemporal, and numerical system model is developed. The accuracy of the model and their ability in determining the effects of several electrical feedbacks on PSOFC during the transient and in the steady state are experimentally validated. Using the validated model, accurate estimations of the impacts of several electrical feedback effects on the performance and durability of the PSOFC PCS is conducted using parametric study. An experimental degradation study is done to estimate the long-term effects of the load transient and the ripple on the performance of the stack. Specifically, we conclude the following:

- The no-load to full-load transient increases the current density in the planar fuel cell abruptly and immediately. The higher level of current density increases the fuel utilization

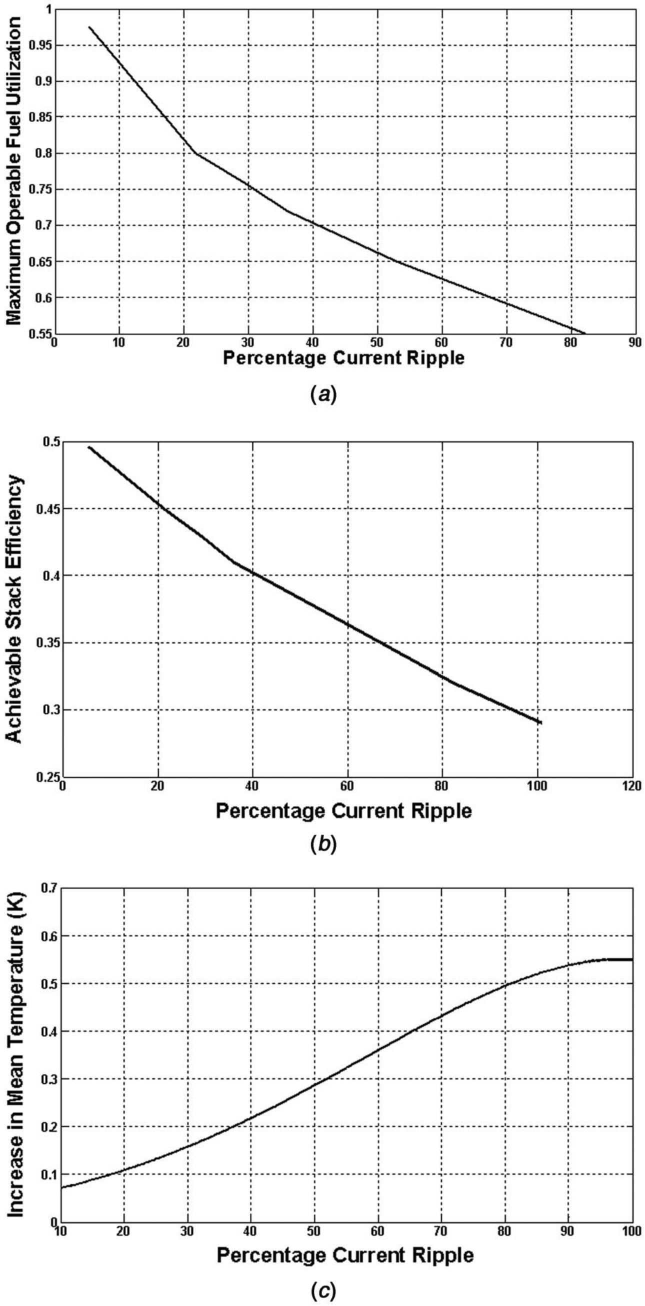

Fig. 15 Effect of low-frequency ripple on (*a*) operable fuel utilization (*b*) achievable efficiency, and (*c*) mean temperature of the stack

and the polarization voltage leading to a drop in the cell voltage. This change in the fuel utilization is detrimental to the cell performance and efficiency.

- The load transient not only increases the mean temperature but also changes the spatial distribution of stack temperature. This variation depends on the magnitude of the current transient and is independent of the slew rate of the transient. The load transients accelerate the degradation of the area specific resistance (ASR) of the planar cell. Therefore, they deteriorate the efficiency of the stack. To prevent this, suitable energy buffering techniques should be available to eliminate the effect of the load transient from the stack.
- The higher ripple current magnitude in the stack current forces to decrease the operating fuel utilization of the stack and, hence, lowers the stack efficiency. However, this has negligible impact on the stack temperature. In the long term, the ripple current accelerates the degradation of the ASR, deteriorating the efficiency of the stack.
- Lower power factor of the load increases the magnitude of current ripple drawn from the stack. And this reduces the efficiency of the stack. The effect of the load power factor on the stack temperature is minimal.

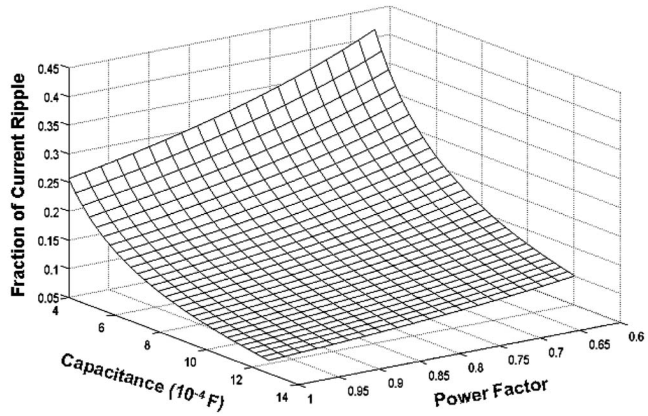

Fig. 16 Effect of power factor of the load on the magnitude of stack current ripple

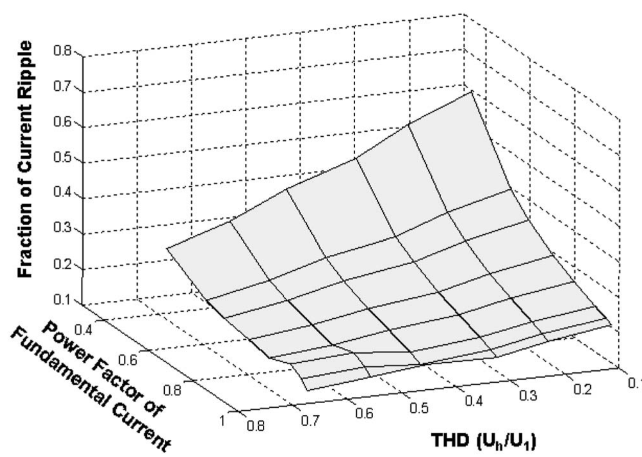

Fig. 17 Effect of THD on the stack current ripple

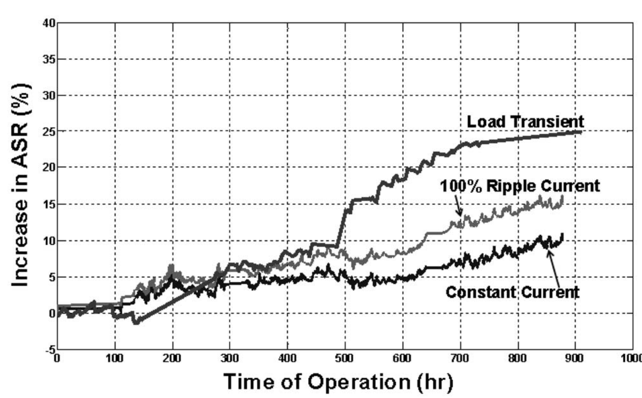

Fig. 18 Comparison of long-term ASR degradation due to low-frequency ripple, constant current, and load transient

Table 1 Stack specifications and test conditions

Number of cells in the stack		25
Cell electroactive area		64 cm^2
Thickness		1.94936 mm
Stack open-circuit voltage		23.75 V
ASR[a] (at 816°C)		1.291 $\Omega\,cm^2$
Fuel composition		$[H_2:H_2O:N_2]$ $=[0.461:0.462:0.077]$
H_2 flow rate		9.54 slpm
N_2 flow rate		1.6 slpm
Airflow rate		38.2 slpm
Air inlet temperature		800°C
Stack core temperature		816°C
Ambient pressure		0.859 atm
Water vapor pressure (76.7°C)		0.397 atm
Calculated ASR constants	A	8.393×10^{-4} $\Omega\,cm^2$
(refer to Eq. (17))	B	8032.32 K
Equiv. cell specific heat (816°C)		627 J kg^{-1} K^{-1}
Equivalent cell density		4491.3 kg m^{-3}

[a]This is the ASR of each of the cells modified to take care of the stack equivalent ASR.

Table 2 PES Specifications

Boost converter	
Inductance (L)	500 μH
Output capacitance (C)	200 μF
Bus voltage	60 V

- Higher THD of the AC load decreases the magnitude of current ripple drawn from the stack. However, it has negligible impact on the stack temperature.

The parametric study in the paper provides a detailed insight into the effects of several electrical-feedback effects on the planar solidoxide fuel cell (PSOFC) stack and the PSOFC power-conditioning system (PCS) as a whole. This will facilitate the design of control and optimization of PSOFC PCS parameters toward the achievement of a highly efficient and reliable power system.

Acknowledgement

This paper was prepared with the support of the U.S. Department of Energy (DOE), under Grant No. DE-FC2602NT41574. However, any opinions, findings, conclusions, or recommendations expressed herein are those of the authors and do not necessarily reflect the views of the DOE. The work herein is also supported in part by the National Science Foundation CAREER Award received by Prof. Mazumder in 2003 under Grant No. 0239131. We acknowledge the help of Mark Timper at Ceramatec for his active assistance during the long-term degradation and transients experimental tests.

Acronyms

PES = power electronics subsystem
PSOFC = planar SOFC
VSI = voltage source inverter
PSOFCS = planar SOFC stack
PCS = power-conditioning system
FL = full load
NL = no load
AL = application load
ASR = area-specific resistance
THD = total harmonic distortion

Appendix A: Specifications and Test Conditions of the Experiment

Table 1 presents the stack specifications and test conditions. The PES specifications are given in Table 2.

Appendix B: Analysis of the Effect of Load Power Factor on the Stack Current Ripple

The current drawn by the inverter from the output of the DC-DC converter, as shown in Fig. 1, can be written using small signal analysis as

$$i_{\mathrm{bus}}=\left(i_{\mathrm{load}}+C_f\frac{dv_f}{dt}\right)d_{\mathrm{vsi}} \tag{B1}$$

where d_{vsi} is the duty ratio of the inverter switches assuming small signal approximation and can be defined as $d_{\mathrm{vsi}}=d_m\sin\omega t$, ω is the frequency of the reference voltage for the inverter. Assuming no phase delay of the output voltage of the inverter with respect to the reference voltage, v_f can be written as $V_m\sin\omega t$. Then assuming stiff bus voltage, Eq. (B1) becomes

$$i_{\mathrm{bus}}=(i_{\mathrm{load}}+\omega V_mC_f\cos\omega t)d_m\sin\omega t \tag{B2}$$

Case A. For a resistive load, $i_{\mathrm{load}}=I_m\sin\omega t$, and Eq. (B2) becomes

$$i_{\mathrm{bus}}=(I_m\sin\omega t+wV_mC_f\cos\omega t)d_m\sin\omega t=\frac{I_md_m}{2}[1-\cos(2\omega t)]+\frac{\omega V_mC_fd_m}{2}\sin(2\omega t) \tag{B3}$$

The filter capacitance being very small, the second term in (B3) is negligible as compared to the first term. The approximate expression for the bus current becomes

$$i_{\mathrm{bus}}=\frac{I_md_m}{2}(1-\cos 2\omega t) \tag{B4}$$

Case B. For a reactive load with power factor, PF$=\cos\phi$, $i_{\mathrm{load}}=I'_m\sin(\omega t+\phi)$. Now for same active power as in case A,

$$\frac{V_mI_m}{2}=\frac{V_mI'_m}{2}\cos\phi\Rightarrow I'_m=\frac{I_m}{\cos\phi} \tag{B5}$$

Now, (B2) becomes

$$\begin{aligned}i_{\mathrm{bus}}(t)&=\left(\frac{I_m}{\cos\phi}\sin(\omega t+\phi)+\omega V_mC_f\cos wt\right)d_m\sin\omega t\\&=\frac{I_md_m}{2}\left(1-\frac{\cos(2\omega t+\phi)}{\cos\phi}\right)+\frac{wV_mC_fd_m}{2}\sin 2\omega t\end{aligned} \tag{B6}$$

Using the same approximation as in (B4), the expression for the bus current becomes

$$i_{\mathrm{bus}}(t)=\frac{I_md_m}{2}[1-A\cos(2\omega t+\phi)] \tag{B7}$$

where $A=1/(\cos\phi)>1$ for all $\phi\neq0$. At the output of the boost converter, assuming constant duty ratio D of the boost converter in the steady state

$$i_{\mathrm{bus}}(t)=(1-D)i_{\mathrm{FC}}(t)-i_C(t) \tag{B8}$$

Assuming a fraction δ of the ripple in the bus current flows in the bus capacitor C,

$$i_C(t)=\frac{I_md_m}{2}(1-\delta)A\cos(2\omega t+\phi) \tag{B9}$$

To allow stiff voltage approximation, the size of the capacitance should be chosen such that, the ripple in the bus voltage is <5%. That is,

$$|\Delta v_{\text{bus}}(t)| = \left| \frac{1}{C}\frac{I_m d_m(1-\delta)A}{2}\int \cos(2\omega t + \phi)dt \right| = \left| \frac{I_m d_m(1-\delta)A}{4\omega C} \right| < 0.05 \times \frac{V_m}{d_m} \tag{B10}$$

Now,

$$(1-D)i_{\text{FC}}(t) = \frac{I_m d_m}{2}(1 - \delta A\cos(2\omega t + \phi)) \tag{B11}$$

$$i_{\text{FC}}(t) = \frac{I_m d_m}{2(1-D)}[1 - \delta A \cos(2\omega t + \phi - k_1)] \tag{B12}$$

Since, $i_{\text{FC}}(t) = I_{\text{FC}} + \hat{i}_{\text{FC}}(t)$, where I_{FC} is the mean stack current and $\hat{i}_{\text{FC}}(t)$ is the ripple component of the stack current. Now the fraction of the ripple in the stack current is given by

$$\frac{\hat{i}_{\text{FC}}(t)}{I_{\text{FC}}} = \frac{\delta}{\cos\phi}\cos(2\omega t + \phi - k_1) \tag{B13}$$

Equation (B11) states that the amplitude of the ripple in the stack current increases with an increase in $|\phi|$. Hence, the ripple current increases with decrease in the load power factor.

Appendix C: Analysis of the Effect of Load Harmonic Distortion on the Stack Current Ripple

Let us consider that the load current contains higher order harmonics (odd order specifically since AC current), then the load current can be explained as

$$i_{h,\text{load}}(t) = \sum_{k=1,3,5\ldots} I_{mk}\sin(k\omega t + \phi_k) \tag{C1}$$

Using (B2) the current drawn by the inverter can be written as

$$i_{\text{bus}}(t) = \frac{d_m}{2}\sum_{k=1,3,5\ldots} I_{mk}\{\cos[(k-1)\omega t + \phi_k] - \cos[(k+1)\omega t + \phi_k]\} + \omega V_m C_f \sin(2\omega t) \tag{C2}$$

The filter capacitance being very small, the second term in (C2) is negligible as compared to the first term for finite load current. Assuming the real power drawn by the harmonic load to be the same as that of a resistive load drawing current with amplitude I_m, then $I_m = I_{m1}\cos\phi_1$. Rewriting (C2) in terms of the fundamental current, I_{m1}

$$\begin{aligned} i_{\text{bus}}(t) &= \frac{I_{m1}d_m}{2}\sum_{k=1,3,5\ldots} c_k\{\cos[(k-1)\omega t + \phi_k] - \cos[(k+1)\omega t + \phi_k]\} \\ &= \frac{I_{m1}d_m}{2}\left[\cos\phi_1 - \left(\cos(2\omega t + \phi_1) - \sum_{k=3,5\ldots} c_k\{\cos[(k-1)\omega t + \phi_k] - \cos[(k+1)\omega t + \phi_k]\}\right)\right] \\ &= \frac{I_m d_m}{2}\left[1 - \frac{1}{\cos\phi_1}\left(\cos(2\omega t + \phi_1) - \sum_{k=3,5\ldots} c_k\{\cos[(k-1)\omega t + \phi_k] - \cos[(k+1)\omega t + \phi_k]\}\right)\right] \end{aligned} \tag{C3}$$

where $c_k = I_{mk}/I_{m1}$ and ϕ_k is described by

$$\phi_k = \cos^{-1}\left(\frac{\cos\phi_1}{\sqrt{k^2(1+\cos^2\phi_1) - \cos^2\phi_1}}\right) \tag{C4}$$

Simplifying (C3), we obtain

$$\begin{aligned} i_{\text{bus}}(t) &= \frac{I_m d_m}{2}\left\{1 - A\sum_{j=2,4,6\ldots}[c_{j-1}\cos(j\omega t + \phi_{j-1}) - c_{j+1}\cos(j\omega t + \phi_{j+1})]\right\} \\ &= \frac{I_m d_m}{2}\left\{1 - A\sum_{j=2,4,6,\ldots}\alpha_j[\cos(j\omega t + \psi_j)]\right\} \end{aligned} \tag{C5}$$

where $A = 1/\cos(\phi_1)$, α_j and ψ_j are given as

$$\alpha_j = \sqrt{c_{j-1}^2 + c_{j+1}^2 - 2c_{j-1}c_{j+1}\cos(\phi_{j+1} - \phi_{j-1})}$$

$$\psi_j = \tan^{-1}\left(\frac{c_{j-1}\sin\phi_{j-1} - c_{j+1}\sin\phi_{j+1}}{c_{j-1}\cos\phi_{j-1} - c_{j+1}\cos\phi_{j+1}}\right) \quad j = 2,4,6,\ldots \tag{C6}$$

At the output of the boost converter, assuming constant duty ratio D of the boost converter in the steady state,

$$i_{\text{bus}}(t) = (1-D)i_{\text{FC}}(t) - i_C(t) \tag{C7}$$

Assuming a fraction of the ripple in the bus current is absorbed in the bus capacitor C,

$$i_C(t) = \frac{I_m d_m A}{2}\sum_{j=2,4,\ldots}(1-\delta_j)\alpha_j\cos(j\omega t + \psi_j) \quad \text{where}$$

$$\delta_j = \frac{2\delta}{j} \text{ for } j = 2,4,6,\ldots \tag{C8}$$

To allow stiff voltage approximation, the size of the capacitance should be chosen such that, the ripple in the bus voltage is $<5\%$. That is,

$$\begin{aligned} |\Delta v_{\text{bus}}(t)| &= \left|\frac{1}{C}\frac{I_m d_m A}{2}\sum_{j=2,4,\ldots}(1-\delta_j)\alpha_j\int\cos(j\omega t + \psi_j)dt\right| \\ &= \left|\frac{I_m d_m A}{2\omega C}\sum_{j=2,4,\ldots}\frac{1-\delta_j}{j}\alpha_j\cos(j\omega t + \psi_j)\right| \\ &< 0.05\frac{V_m}{d_m} \end{aligned} \tag{C9}$$

Now,

$$(1-D)i_{\text{FC}}(t) = \frac{I_m d_m}{2}\left[1 - A\sum_{j=2,4,\ldots}\delta_j\alpha_j\cos(j\omega t + \psi_j)\right] \tag{C10}$$

$$i_{\text{FC}}(t) = \frac{I_m d_m}{2(1-D)}\left[1 - 2A\delta\sum_{j=2,4,\ldots}\frac{\alpha_j}{j}\cos(j\omega t + \psi_j)\right] \tag{C11}$$

Since, $i_{\text{FC}}(t) = I_{\text{FC}} + \hat{i}_{\text{FC}}(t)$, where I_{FC} is the mean stack current and $\hat{i}_{\text{FC}}(t)$ is the ripple component of the stack current. Now the fraction of the ripple in the stack current is given by

$$\frac{\hat{i}_{\text{FC}}(t)}{I_{\text{FC}}} = \frac{\delta}{\cos\phi_1}\sum_{j=2,4,\ldots} a_j\cos(j\omega t + \psi_j) \quad \text{where}$$

$$a_j = \frac{2\alpha_j}{j}, \quad j = 2,4,6,\ldots \tag{C12}$$

Equation (C12) states that the amplitude of the ripple in the stack current increases with an increase in $|\phi_1|$. Again this ripple is dependent on α_j and ψ_j (Eq. (C8)), which depend on the fraction of the harmonic components c_j and their frequencies, $j\omega$.

Now let us consider the harmonic current consists of only third and fifth harmonics.

Case I. Let us assume, $c_3=0.2$, $c_5=0.11$, and $\phi_1=0.4$. Then, $\phi_3=0.903$ and $\phi_5=1.13$ radians and THD=0.228. From (C6) $\alpha_2=0.8304$, $\psi_2=0.284$, $\alpha_4=0.096$, $\psi_4=0.642$, $\alpha_6=0.11$, and $\psi_6=1.13$. Using the following values, the fraction of the ripple in the bus current is found to be 0.995 to that of the mean bus current. With $\delta=0.2$, and the ripple in stack current is 0.193.

Case II. Let us assume, $c_3=0.5$, $c_5=0.24$, and $\phi_1=0.4$. Then $\phi_3=0.903$ and $\phi_5=1.13$ radians and THD=0.554. From (C6) $\alpha_2=0.611$, $\psi_2=-0.005$, $\alpha_4=0.272$, $\psi_4=0.703$, $\alpha_6=0.24$, and $\psi_6=1.13$. Using these values, with $\delta=0.2$ and using (C12), the fraction of the ripple in the stack current is 0.188.

From above two cases, we observe the ripple in the stack current decreases with an increase in the THD for a particular power factor of the fundamental current cos ϕ_1.

References

[1] Lasher, S., 2003, "Assessment of Fuel Cells as Auxiliary Power Systems for Transportation Vehicles," Hydrogen and Fuel Cells Merit Review Meeting, Berkeley, CA, http://www1.eere.energy.gov/hydrogenandfuelcells/pdfs/merit03/90_tiax_steven_lasher.pdf.

[2] Hsiao, Y. C., and Selman, J. R., 1997, "The Degradation of SOFC Electrodes," Solid State Ionics, **98**, pp. 33–38.

[3] Huang, X., and Reifsnider, K., 2001, "Modeling Long-Term Performance of Solid Oxide Fuel Cells: A Phenomenological Approach," 15th Annual Conference of Fossil Energy Materials, Knoxville.

[4] Achenbach, E., 1995, "Response of a Solid Oxide Fuel Cell to Load Change," J. Power Sources, **57**, pp. 105–109.

[5] Hartvigsen, J., Elangovan, S., and Khandkar, A., 1993, *Science and Technology of Zirconia V*, Badwal, S., Bannister, M., and Hannink, R., eds., Technomic, Lancaster.

[6] Acharya, K., Mazumder, S. K., Burra, R. K., Williams, R., and Haynes, C. L., 2003, "System-Interaction Analyses of Solid Oxide Fuel Cell (SOFC) Power-Conditioning System," *Proceedings of the IEEE IAS Conference*, pp. 2026–2032.

[7] Acharya, K., Mazumder, S. K., and Burra, R. K., 2004, "Impact of Power-Electronics Systems on the Performance and Durability of Tubular Solid-Oxide Fuel Cell," *Proc. of IEEE Applied Power Electronics Conference*, IEEE, New York, Vol. 3, pp. 1515–1520.

[8] Mazumder, S. K., Acharya, K., Haynes, C. L., Williams, R., von Spakovsky, M. R., Nelson, D. J., Rancruel, D. F., Hartvigsen, J., and Gemmen, R. S., 2004, "Solid-Oxide-Fuel-Cell Performance and Durability: Resolution of the Effects of Power-Conditioning Systems and Application Load," IEEE Trans. Power Electron., **19**, pp. 1263–1278.

[9] Gemmen, R. S., 2003, "Analysis for the Effect of Inverter Ripple Current on Fuel Cell Operating Condition," ASME J. Fluids Eng., **125**(3), pp. 576–585.

[10] Ferguson, J. R., Fiard, J. M., and Herbin, R., 1996, "A Mathematical Model of Solid Oxide Fuel Cells," J. Power Sources, **58**, pp. 109–122.

[11] Yentekakis, I. V., Neophytides, S., Seimanides, S., and Vayenas, C. G., 1993, "Mathematical Modeling of Cross-Flow, Counter-Flow and Cocurrent-Flow Solid Oxide Fuel Cells: Theory and Some Preliminary Experiments," *Proc. of 2nd Int. Symposium on Solid Oxide Fuel Cells*, Athens, Official Publication of the EEC, Luxembourg, pp. 281–288.

[12] Erdle, E., Gross, J., Muller, H. G., Müller, W. J. C., Reusch, H. J., and Sonnenschein, R., 1991, *Proceedings of 2nd International Symposium on SOFCs*, Singhal et al., eds., pp. 265–267.

[13] Ferguson, J. R., 1991, Analysis of Temperature and Current Distributions in Planar SOFC Designs, *Proceedings of 2nd International Symposium on SOFCs*, Singhal et al., eds., pp. 305–309.

[14] Hendrikson, P. V., 1994, 2nd Nordic Symposium on High Temperature Fuel Cells, Nordby, T., and Poulsen, F. W., eds., The Nordic Energy Research Programme and University of Oslo, Norway.

[15] Constantinides, A., and Mostoufi, N., 1999, *Numerical Methods for Chemical Engineers With Matlab Applications*, Prentice Hall, Englewood Cliffs, NJ.

[16] Erickson, R. W., and Maksimovic, D., 2004, *Fundamentals of Power Electronics*, 2nd ed., Kluwer, Dordrecht.

[17] Lee, F. C., 1990, *Modeling, Analysis, and Design of PWM Converter*, Virginia Power Electronic Center Publications Series, Blacksburg, VA.